Fuel 298 (2021) 120671

Contents lists available at ScienceDirect

Fuel

journal homepage: www.elsevier.com/locate/fuel

Full Length Article

Impact dynamics and morphology of urea-water-solution droplets impinging on a hot plate under urea-SCR relevant conditions: Influence of surface tension

Aniket P. Kulkarni [a,*], Thanos Megaritis [a], Lionel Christopher Ganippa [a]

[a] College of Engineering Design and Physical Sciences, Brunel University London, Uxbridge UB8 3PH, United Kingdom

ARTICLE INFO

Keywords:
Urea water solution
Fuel droplet impact
Selective catalytic reduction (SCR) system
Droplet Spreading dynamics
Dropsize distribution
Surface tension

ABSTRACT

NO_x conversion efficiency of urea-selective-catalytic reduction (SCR) systems are governed by dispersion of urea-water-solution (UWS) injected in exhaust manifold. Impingement of larger size urea droplets on mixture distribution fans as well as to the internal surfaces of SCR systems will lead to formation of deposits, which has potential to deteriorate the effectiveness of urea-SCR system. In this work, detailed analyses on droplet-wall interactions of UWS droplets impinging on a hot plate under urea-SCR-relevant conditions have been presented. The effect of lowering surface tension of UWS on droplet morphology and impact dynamics were also explored. The surface tension of UWS was lowered from 73.7 to 30.2 mN/m by adding a surfactant (DDA75).

Distinct modes of droplet impact viz., deposition, thermal atomization, rebound and breakup were identified. The DDA75 droplets showed a significant increase in maximum spreading factor (β_{max}) by 37% due to 59% reduction in surface tension. New empirical correlation was developed to predict β_{max} for UWS and DDA75 droplets, which considers the effect of wall temperature on spreading process; the predicted β_{max} values for different liquids including water, hydrocarbon and alternative fuels viz., n-heptane, n-decane, Jatropha biodiesel and camelina-based alternative jet-fuel had a mean error less than 8.2% across all wall temperature conditions. The drop-size distributions of secondary DDA75 droplets revealed considerably narrower drop-size distribution (up to 36%) compared to UWS droplets. The surfactant-added-UWS droplets have the potential to enhance NO_x reduction in SCR systems through better evaporation and mixing and also through reduction in the formation of urea deposits.

1. Introduction

Stringent emission norms demand effective after-treatment devices for power generators. Selective catalytic reduction (SCR) systems are commonly employed to mitigate combustion generated nitrogen oxides (NO_x) emissions. The SCR systems in engines rely on on-board generation of ammonia and its mixing with the engine exhaust in the presence of a catalyst [1,2]. This is accomplished by injecting aqueous solution of urea (32.5% by weight, also called as adblue or urea-water solution, UWS) in the exhaust manifold of engines [3,2,4]. The injected UWS undergoes a series of physical and chemical processes including evaporation, thermolysis and hydrolysis to produce ammonia as reducing agent in the SCR system [1,5–8]. The NO_x conversion efficiency of SCR system mainly depends on mixing of UWS with the exhaust gases, which is governed by performance of mixers and the interaction between UWS spray and the exhaust gases [1,9–11,6,7,12]. The mixers are employed in the exhaust manifold to aid the mixing of UWS, where UWS droplets impinge on the hot walls of the mixers [13–15]. The interactions between UWS droplets and mixer blades have significant influence on the resultant mixing [16]. The overall process efficiency also depends on the inevitable interactions of UWS droplets with the walls of the SCR systems, which might result in urea wall residues [17,18]. The formation of urea wall residues impairs NO_x conversion efficiency and increases back-pressure in the exhaust manifold that leads to an adverse impact on combustion efficiency and engine emissions [1,7,11,6,12,17]. Thus, the interactions of large UWS droplets on hot surfaces impairs mixing of UWS with the engine exhaust that leads to the formation of urea wall residues and thereby affecting the overall performance of urea-SCR systems. Hence, it is important to study the interaction of UWS droplets on a hot metal surface under SCR-relevant conditions to gain an

* Corresponding author.
E-mail address: aniket.kulkarni@brunel.ac.uk (A.P. Kulkarni).

https://doi.org/10.1016/j.fuel.2021.120671
Received 25 November 2020; Received in revised form 9 March 2021; Accepted 13 March 2021
Available online 17 April 2021

understanding of how the droplet interactions affects NO*x* conversion efficiency and that impairs urea wall residues.

Single droplet studies are commonly preferred to gain deeper understanding of droplet-wall interaction, which becomes difficult in case of studies using sprays or droplet-chains due to a large number of droplets [19–21]. Extensive research have been carried out on the interactions of single droplets with hot solid walls [19–26]. Most of these studies have focused on droplets of single component liquids (e.g. water [22,23,25,27], ethanol, n-heptane, n-dodecane [26,28] etc.). Few studies have reported experimental outcomes of interaction of binary urea-water-solution droplets with a hot wall [29–32], a cold-wall [24], a film of UWS [33,34]. In the pioneering work, Birkhold et al. [29,31] studied the impingement of micrometric UWS droplets on a heated aluminum plate using a droplet chain generator that produced UWS droplets of diameter 90 μm to 180 μm with impact velocities from 5 m/s to 20 m/s. The experimental observations were used to propose a regime map of the outcomes for wall temperatures below 167 °C (expressed in terms of T*, ratio of wall temperature to saturation temperature of UWS) and splashing parameter K, which is a function of droplet Reynolds number and Weber number. Bornhorst and Deutchmann [31] studied single droplet impingement of UWS droplets on a stainless steel plate for wall temperatures from 84 °C to 310 °C. They studied impact morphology of UWS droplets under different impact velocity conditions (1.2 to 4 m/s), outcomes of the impact presented in the regime map for wall temperatures below 167 °C in terms of T* and the splashing parameter K was in-line with the findings of Birkhold [29]. Quissek et al. [32] studied the effect of impingement angles of UWS droplets on the outcome of the impact using a droplet chain generator that produced droplets of diameters from 220 μm to 420 μm at different droplet velocities from 1.6 m/s to 7.7 m/s. Two impingement angles viz., 30° and 70° were considered, but the impingement angle had no major influence in their proposed regime map for wall temperatures from 80 °C to 360 °C and found that the regime map was consistent with those reported by Bornhorst and Deutchmann [31] and Birkhold [29]. These studies have focused on droplet morphology, without accounting for impact dynamics of UWS droplets. Recently, impact dynamics of UWS droplets impinging on a stainless steel plate was studied at room temperature to investigate the effect of impact velocity on instantaneous spreading factor and maximum spreading factor (β_{max}) [24]. The experimental β_{max} values were compared with the predicted β_{max} values from various correlations, the experimental β_{max} values were in agreement with the empirical correlation of Scheller and Bousfield [24]. However, the temperature of the stainless steel plate was fixed at room temperature and the effect of wall temperature on droplet spreading dynamics was not explored in [24]. Thus, it is important to understand droplet morphology and impact dynamics of binary UWS droplets under urea-SCR relevant conditions.

The droplet impact dynamics and outcomes of the impact can be altered by changing physical properties of the liquid viz., viscosity or surface tension [22,35,27,36–41]. The spreading dynamics of water droplets have been extensively studied for varying surface tension values by adding different surfactants [22,27,36]. It was observed that the droplets of surfactant-added water solutions generally exhibit higher values of instantaneous spreading factor (β) and maximum spreading factor (β_{max}) due to the reduction in surface tension of water [22,27,36,37]. Bertola [35] observed that the addition of small quantity of polymer additive suppressed the capillary effect that leads to the formation of secondary droplets, which can be used as a criterion to define the dynamic Leidenfrost temperature during the drop impact. Thus, they concluded that the dynamic Leidenfrost temperature can be lowered with the addition of the polymer additive to water. Qiao and Chandra [22] studied the effect of lowering surface tension of water on Leidenfrost temperature. They added sodium dodecyl sulphate (SDS) surfactant to water with a concentration of 1000 ppm by weight of the surfactant, which lowered surface tension of water from 73.5 to 50 mN/m. It was demonstrated that the use of surfactant has potential to reduce Leidenfrost temperature of water droplets impacting on a heated plate. In urea-SCR systems, lowering Leidenfrost temperature of UWS might help in minimizing physical contact between UWS droplets and the walls, which might help in reducing wall residues. Moreover, it was observed that addition of surfactant to UWS has potential to improve NO_x conversion efficiency and to reduce urea wall residues in SCR systems [14,42,43]. Thus, it is important to understand the droplet morphology and impact dynamics of UWS droplets impinging on a hot plate under urea-SCR relevant conditions, particularly for lower surface tension value of UWS as not much work has been reported to explore the interactions of UWS and surfactant added UWS droplets (i.e. DDA75) with a plate at elevated temperatures.

This study presents analyses on droplet-wall interaction of a UWS droplet impinging on a hot plate under urea-SCR relevant temperature conditions. The effect of lowering surface tension of UWS on droplet morphology and impact dynamics viz., spreading factor, maximum spreading factor and drop-size distributions of secondary droplets have been explored under a wide range of impact momentum and wall temperature conditions. A combined regime map of the outcomes of impact dynamics for UWS and surfactant added UWS (i.e. DDA75) under urea-SCR relevant conditions have been corroborated on a regime diagram, based on this new simplified correlation to predict maximum spreading factor of the UWS droplets has been proposed.

2. Experimental setup and methodology

This section presents details on experimental setup and image processing methods. Also, the description on preparation of test liquids, their physical properties, test procedures and experimental conditions have been provided.

2.1. Experimental setup

Fig. 1 shows schematic of experimental setup used in the present work. The experimental setup consists of a stainless steel plate with the heating controller, a droplet generating arrangement and a high-speed imaging system. A stainless steel plate of (62 mm x 48 mm and 4 mm thick) was used as the test target. A cartridge heater was snug-fitted in the plate and was controlled by a PID controller. Temperature of the plate was monitored at a location just below the of drop impact using a K-type thermocouple which was placed 2 mm below the top surface of the target plate. This arrangement ensured that temperature (T_s) at the top surface of target plate was controlled as per the designed test conditions. The measurements were carried out after ensuring that T_s had reached the desired steady-state value.

The droplets were generated using a micro-pipette and micro-tips. This gravity-controlled method generated droplets with diameter 2.15 mm with the standard deviation of 0.051 mm for both, UWS and DDA75 droplets. The height of micro-tip (H) from the plate was changed to vary the impact velocity as shown in Fig. 1. Impact velocity was calculated using free fall velocity, obtained by comparing the potential and kinetic energies of the droplet.

Droplet impact events on the hot plate were recorded using high speed shadowgraph method. The droplet was back-illuminated using an LED light source and a diffuser sheet. A high-speed camera (Photron FASTCAM, SAX2) was used to capture evolution of the droplet impact events. The images were acquired at 3000 fps with shutter exposure of 38 μs and pixel resolution of 27.78 μm per pixel. This optical arrangement provided the field of view of 768 pixel x 464 pixel (i.e. 21.33 mm x 12.9 mm) which enabled to capture complete series of post-impact events, including secondary droplets.

2.2. Image processing

The images were analyzed using image processing tools to extract various parameters associated with droplet impact and size distributions

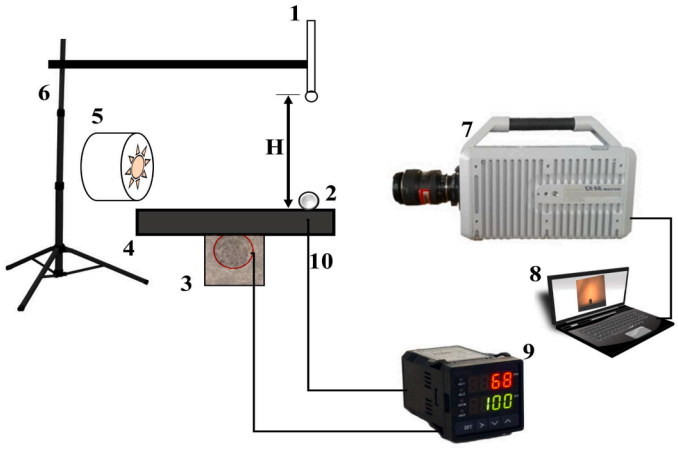

1. Droplet generator 2. UWS droplet 3. Cartridge heater 4. Target plate 5. Back-light illumination 6. Stand 7. high speed camera with objective lens 8. Computer 9. PID temperature controller 10. K-type thermocouple

Fig. 1. Schematic of experimental setup to study impact dynamics of UWS and DDA75 droplets under different temperature conditions using high-speed shadowgraph imaging.

of the secondary droplets as shown in Fig. 2. The droplet spreading factors (β) and maximum spreading factors (β_{max}) were calculated by measuring the instantaneous maximum extent of the spreading lamella (D_i). The images were processed using the median filter and image subtraction. Binary images were obtained by using a global thresholding method and the subtracted images. The binary images along with an edge detection algorithm were used to calculateD_i, which was normalized with the initial droplet diameter (D_0) to get the temporal variation of the spreading factors ($\beta=\frac{D_i}{D_0}$) as shown in Fig. 2(a). Drop-size distributions of secondary droplets were obtained using an in-house developed MATLAB code. The background subtracted images were binarised using a global thresholding method, the sizes of droplets were determined using image segmentation and the pixel resolution. The obtained drop-size distributions were normalized with droplet diameter before impact (D_0). Out-of-focus droplets and droplets with sphericity less than 0.8 were neglected to minimize the error in drop-size measurements as shown in Fig. 2(b) [44,45]. More than ten events were considered for each drop-size measurement condition, which ensured the presence of sufficient number of droplets in drop-size distributions. Since the resolution of the images was 27.7 μm per pixel, fine mist-like droplets in thermal atomization regime were not considered for the drop-size distributions to avoid diffraction limit of the optical system and to ensure reliable drop-size measurements [44].

2.3. Test liquids and physical properties

This work was carried out by using the commercially available urea-water-solution (32.5% urea in water on mass basis). The surfactant N,N, Dimethyldodecylamine N-oxide (DDA) was used in the present work to lower the surface tension of UWS. This surfactant was selected based on our previous investigation [46] that revealed improvement in atomization of UWS and the past studies which reported improvements in NO_0 conversion efficiency while using this surfactant in urea-SCR systems [42,43,47]. The surfactant was added 75% of its critical miscelle concentration (CMC) in UWS to prepare surfactant-added UWS (DDA75) and this corresponds to 0.3% whilst the CMC of DDA surfactant in UWS was determined as 4 ml per liter using the surface tension method [46]. In this method, surface tension values of UWS were measured using the pendent-drop method (First Ten Angstroms, FTA100) at different concentrations as shown in Fig. 3.

2.3.1. Physical properties of the test liquids

The physical properties of the test liquids were measured at room

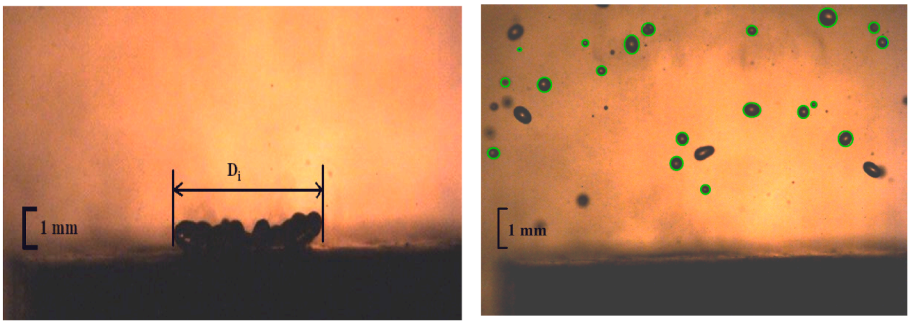

(a) Instantaneous droplet diameter (D_i) in the calculation of spreading factors (β) and maximum spreading factor (β_{max})

(b) Secondary droplets detected with the image processing methods for the drop-size distributions

Fig. 2. Definition of instantaneous droplet diameter (D_i) in the calculation of spreading factors and an example of image processing of secondary droplets to obtain drop-size distributions.

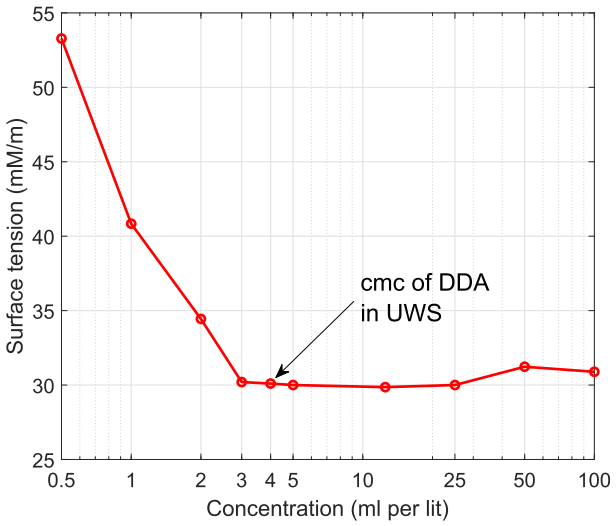

Fig. 3. Surface tension values of UWS for various concentrations of DDA surfactant. Critical micelle concentration (cmc) of DDA in UWS was determined as 4 ml per liter using the pendant drop method of surface tension measurement [46].

temperature of 20 °C. The surface tension measurements were carried out using pendent-drop method (First Ten Angstroms, FTA100), the measurements were calibrated using deionized water as a standard liquid. Minimum ten measurements were performed at each test condition, and standard deviation and mean standard error was calculated as shown in Table 1. The maximum mean standard error in the surface tension measurements was less than 1.3%. Surface tension (σ_l) of UWS reduced significantly, minimum value of 30.2 mN/m was observed with DDA surfactant with the concentration of 75% of CMC (i.e. DDA75). Dynamic viscosity (μ_l) was measured using a rolling ball viscometer (Anton Paar, AMVn). Density (ρ_l) was determined using a high-precision weighing machine. The values of μ_l and ρ_l for UWS were 1.41 mPa.s and 1066.3 kg/m^3, while those for DDA75 were 1.42 mPa.s and 1070.3 kg/m^3, respectively. Thus, the addition of surfactants has marginal influence on dynamic viscosity and density of the UWS. Saturation temperature (T_{sat}) of UWS at ambient pressure was 104.2 °C [31,24].

2.4. Test conditions

Droplet spreading dynamics and droplet morphology were studied under different wall temperature and impact momentum conditions. The wall temperature was varied from 110 °C to 300 °C. This range of wall temperatures was expected to cover entire range of thermodynamic events occurring in the urea-SCR system. Two liquids were considered in the present experiments viz., UWS and surfactant added UWS (DDA75) to explore the influence of lowering surface tension of UWS. Droplet impact momentum was varied by changing the height of impact (H) as 5.2 cm, 11.5 cm, 20.5 cm and 32.5 cm. These distances resulted in free fall velocities of 1, 1.5, 2.5 and 2 m/s, respectively. The standard deviation in U_o was less than 0.1 m/s and it was also confirmed from the high-speed imaging. The corresponding droplet Reynolds number ($Re = \frac{\rho_l U_0 D_0}{\mu_l}$) and droplet Weber numbers ($We = \frac{\rho_l U_0^2 D_0}{\sigma_l}$) were calculated using

Table 1
Surface tension values of the UWS and surfactant-added UWS at room temperature [46].

	UWS	DDA75
Surface tension ($\sigma_l, mN/m$)	73.7	30.2
Standard deviation (mN/m)	1.18	0.95
Mean standard error (%)	0.54	1.29

the physical properties of UWS and DDA75 droplets at 20 °C. The experimental conditions explored in the current study have been summarized in Table 2. The mean surface roughness (R_a) of the plate was measured using a Perthometer and was observed to be in the range of 1.35 −1.74 μm. Outcomes of the impact, droplet spreading dynamics viz., instantaneous spreading factors (β), maximum spreading factors (β_{max}), and drop-size distributions of secondary droplets were studied for the wide range of operating conditions relevant to urea-SCR systems.

3. Results and discussion

This section presents the findings of droplet impact on flat plate of varying surface temperature, droplet impact velocity, change in surface tension of UWS and all of these effects on droplet morphology and dynamics associated with dispersion and breakup under wide operating conditions.

3.1. Droplet morphology and regime map

For the wide range of test conditions (Table 2) considered in this work, different impact modes were identified for UWS and DDA75 droplets based on the surface temperature (T_s), surface tension of UWS and droplet impact momentum as shown in Fig. 4. The modes can be broadly classified as deposition (A), rebound (B) and secondary breakup (C), these modes can be further subdivided based on the occurrence of thermal atomization. Deposition mode was observed at low wall temperature conditions (T_s = 110 °C and 150 °C) for both UWS and DDA75 droplets, where the droplet remains attached to the wall without any further movement as shown in Fig. 4(b)–(d) and (f)–(h). The droplet experiences nucleate boiling along with foaming as can be seen in Fig. 4 (c) and (d), ultimately results in urea residues on the plate. Thus, deposition mode (A) is undesirable in urea-SCR systems due to potential urea wall residues. In the rebound mode (B), a vapor film formed between spreading lamella and the plate which levitated the lamella. The vapor layer prevents direct interaction between the surface and the liquid, which is also referred to as Leidenfrost effect as can be observed in Fig. 4(k) and (l) and Fig. 4(n)–(p). The lamella later congregated into a shape of a droplet (of similar order of the parent droplet) due to high surface tension and low impact momentum of the parent droplet and this mode was observed under B2 condition of wall temperatures of the order 300 °C for UWS droplets. In secondary breakup mode (C), breakup of the spreading lamella was observed under higher temperatures (>200 °C) and higher impact momentum conditions. The spreading lamella disintegrated into a number of small droplets, showing secondary atomization of the lamella as can be seen in Fig. 4(r)–(t) and (v)–(x).

Thermal atomization in UWS droplets was observed for wall temperatures between 150 °C < T_s<250 °C (e.g. Fig. 4(j)–(l)). Thermal atomization can be described as the ejection of fine mist-like droplets from the surface of droplet impinging on a hot plate as can be observed in Fig. 4(j)–(l), (r) and (s). The heat transfer effect during droplet-wall interaction causes vapor bubbles to be formed within the droplet,

Table 2
Summary of the test conditions.

Parameter	Range	
	UWS	DDA75
Initial droplet diameter (D_0, mm)	2.15±0.051	
Droplet velocity before impact (U_0, m/s)	1, 1.5, 2 and 2.5	
Wall temperature (T_s, °C)	110, 150, 200, 250 and 300	
Reynold's number, *Re*	1627 to 3990	
Surface tension, (σ, mN/m)	73.7	30.2
Weber number, *We*	31.1 to 194.36	73.8 to 461.26
Splashing parameter ($K = Re^{0.25}We^{0.5}$, [29,30,48])	35.42 to 110.8	54.56 to 170.69

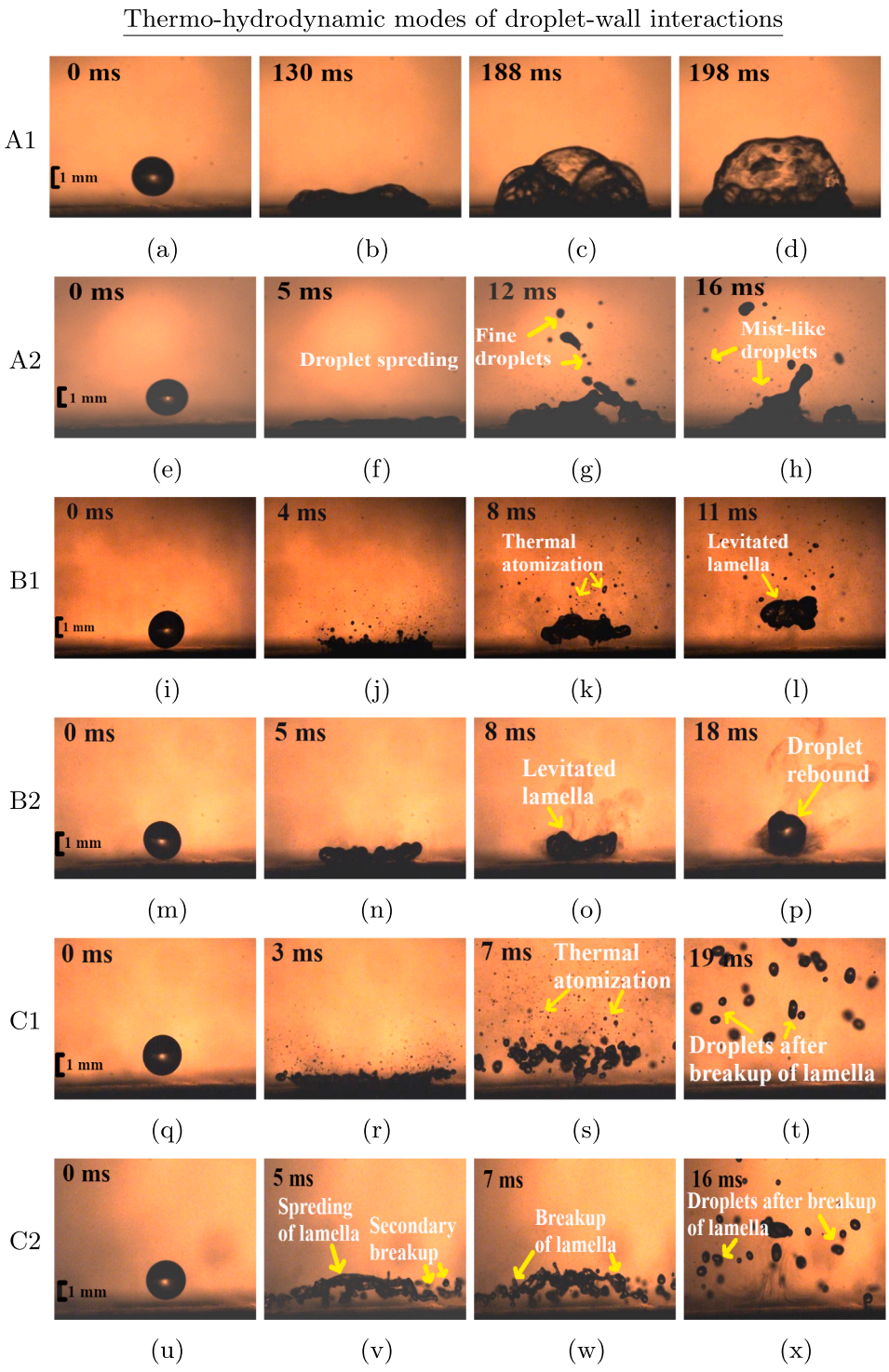

Fig. 4. Various outcomes of the impact of UWS and DDA75 droplets on a hot plate under different impact momentum and wall temperature conditions. Six distinct modes were observed: A1: Deposition; (UWS, *Re* = 3990; T*s* = 110 °C), A2: Deposition with thermal atomization; (DDA75, *Re* = 3990; T*s* = 150 °C), B1: Rebound with thermal atomization; (UWS, *Re* = 1627; T*s* = 200 °C), B2: Rebound without thermal atomization; (UWS, *Re* = 1627; T*s* = 300 °C), C1: Lamella levitation and breakup with thermal atomization; (UWS, *Re* = 3990; T*s* = 200 °C), C2: Lamella levitation and breakup without thermal atomization; (DDA75, *Re* = 3990; T*s* = 250 °C.).

which burst at the free surface of the droplet due to difference in vapor pressure, resulting in ejection of fine mist-like droplets [25,49]. Thermal atomization in DDA75 droplets was observed in the range of 150 °C < T_s<200 °C (e.g. Fig. 4(f)–4(h)) with no thermal atomization for wall temperatures of 250 °C and 300 °C as shown in Fig. 4(v)–(x) and in Fig. 5. This might be attributed to the reduction in surface tension of DDA75, which might have impeded the formation and ejection of vapour bubbles due to detached lamella and inhibited thermal atomization in DDA75 droplets. This observation corroborates with that reported in Bertola et al. [35,50], where they observed reduction in maximum wall temperature for thermal atomization due to addition of an additive to water.

The events of wall-droplet interaction for UWS and DDA75 droplets have been summarized in a regime map for varying impact momentum (i.e. *Re* number) and wall temperature as shown in Fig. 5. It was observed that *Re* number has no significant influence on the occurrence of thermal atomization, whereas the reduction in surface tension has altered the range of wall temperature for occurrence of thermal atomization in UWS. The outcomes of the wall-droplet interactions were further simplified using a conceptual regime map as shown in Fig. 6. The deposition mode (A) occurs at wall temperatures below 150 °C ($T_{deposition}$<150 °C) for UWS and DDA75 droplets, further increase in wall

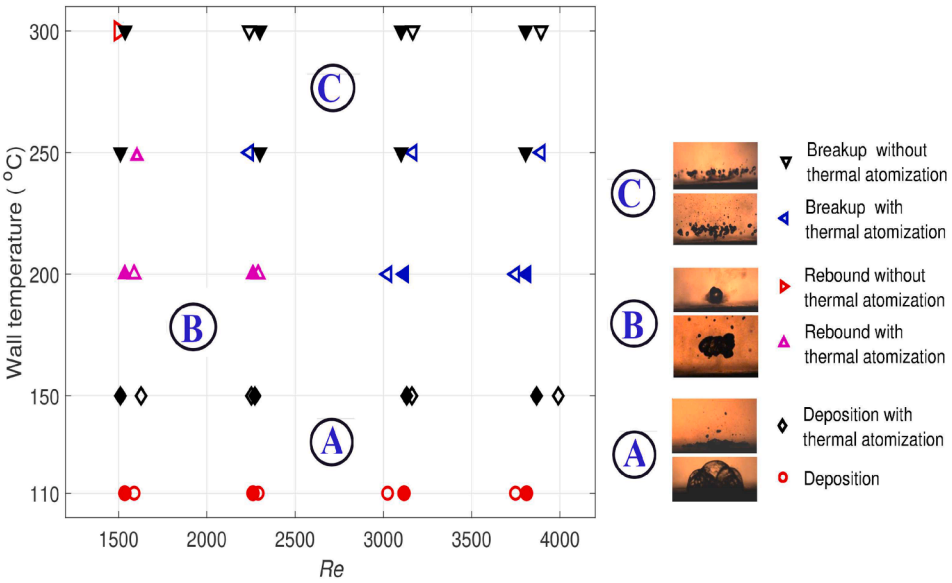

Fig. 5. Regime map of UWS and surfactant-added UWS droplets for varying *Re* and wall temperature T_s, where six distinct modes were observed. Filled symbols represent DDA75 droplets while open symbols represent UWS droplets.

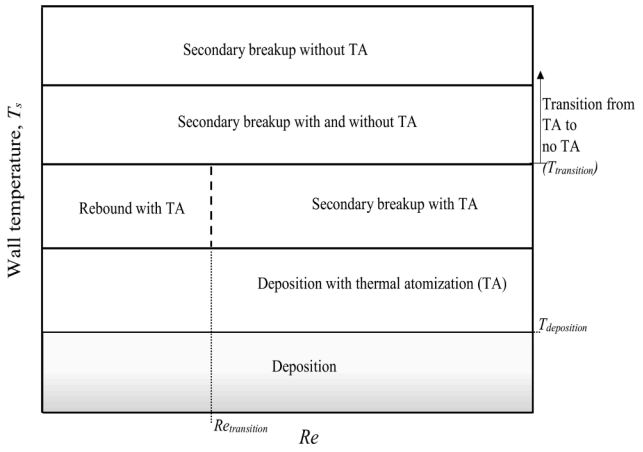

Fig. 6. Conceptual regime map for UWS and DDA75 droplets impacting on a hot plate.

temperature showed transition from thermal atomization to no thermal atomization. The increase in impact momentum ($Re > Re_{transition}$) results in rebound or breakup of levitating lamella under wall temperature conditions above $T_{deposition}$ as shown in Fig. 6.

3.2. Temporal variation of spreading factors ($\beta = \frac{D_L}{D_0}$)

Dynamics of a droplet impacting on a solid wall can be divided into three parts - instantaneous droplet spreading, maximum spreading and droplet retraction i.e. droplet receding or recoil. The effect of surface tension of UWS and wall temperature on the impact dynamics of the UWS droplets have been examined under a range of droplet impact momentum conditions. The spreading factors (β) were obtained by measuring the instantaneous maximum extent of the liquid lamella (D_i) as described in Section 2.2. Fig. 7 shows variations of spreading factors of UWS and DDA75 droplets for wall temperatures of 110 °C, 200 °C, 250 °C and 300 °C, respectively.

It was observed that the spreading rates of UWS and DDA75 droplets were strongly dependent on droplet *Re* and wall temperature (T_s) as shown in Fig. 7(a)–(d). The increase in *Re* and wall temperature favoured lamella spreading and resulted in higher spreading factors (β) due to a higher radial spreading velocity for both UWS and DDA75 droplets. The maximum spreading of the UWS droplets for the $Re = 1627$ case was observed near 5.7 ms for $T_s =$ 110 °C condition (Fig. 7(a)), while it occurred near 2.1 ms for the higher *Re* condition ($Re = 3990$), which implies the increase in spreading velocity with an increase in *Re*. These observations are in-line with those reported in literature on impacting fuel droplets [26,51,52]. Further, the effect of addition of surfactant to UWS on β was dependent on the wall temperatures. At low wall temperature of $T_s = 110$ °C, the droplet spreading was marginally influenced by the reduction in the surface tension of UWS with a small increase of around 3.5%. On the other hand, lower surface tension of DDA75 droplet favoured lamella spreading under higher wall temperatures, the significant increase by up to 38% at $T_s = 250$ °C) in the maximum spreading factor was observed at the high *Re* number condition ($Re = 3990$), similar increase was also seen in Fig. 7(c) and (d). This might be attributed to the combination of lower frictional forces experienced by the spreading lamella due to presence of the vapour film and the lower surface tension of DDA75, which resulted in significantly higher spreading factors. The higher spreading of DDA75 droplets might favour evaporation and subsequent heat and mass transfer processes at the walls or surface of a mixer due to larger surface area available along the liquid-solid interface and might improve mixing of UWS in SCR systems.

The droplet receding or recoil refers to the decrease in maximum spreading of the liquid lamella. The droplet receding was minimal after the time interval of around 6 ms for wall temperature of 110° as shown in Fig. 7(a). This indicates the absence of further movement of the liquid lamella due to the perfect contact between the wall surface and the liquid, which restricts the movement of the lamella. This condition also implies that the vapor film, which lifts the liquid lamella due to Leidenfrost phenomenon has not been formed yet for this wall temperature and it might lead to nucleate boiling regime. Therefore, restricted movement of liquid lamella leads to minimal droplet receding and this causes undesirable urea wall-residues in mixer fans as well as SCR systems maintained at relatively low wall temperatures. The droplet receding was more prominent under wall temperatures above 200 °C as can be seen in Fig. 7(b)–(d). Under these wall temperature conditions, the Leidenfrost behavior, which detaches the spreading lamella from the wall due to the presence of vapor layer, was observed that might also favour the droplet receding.

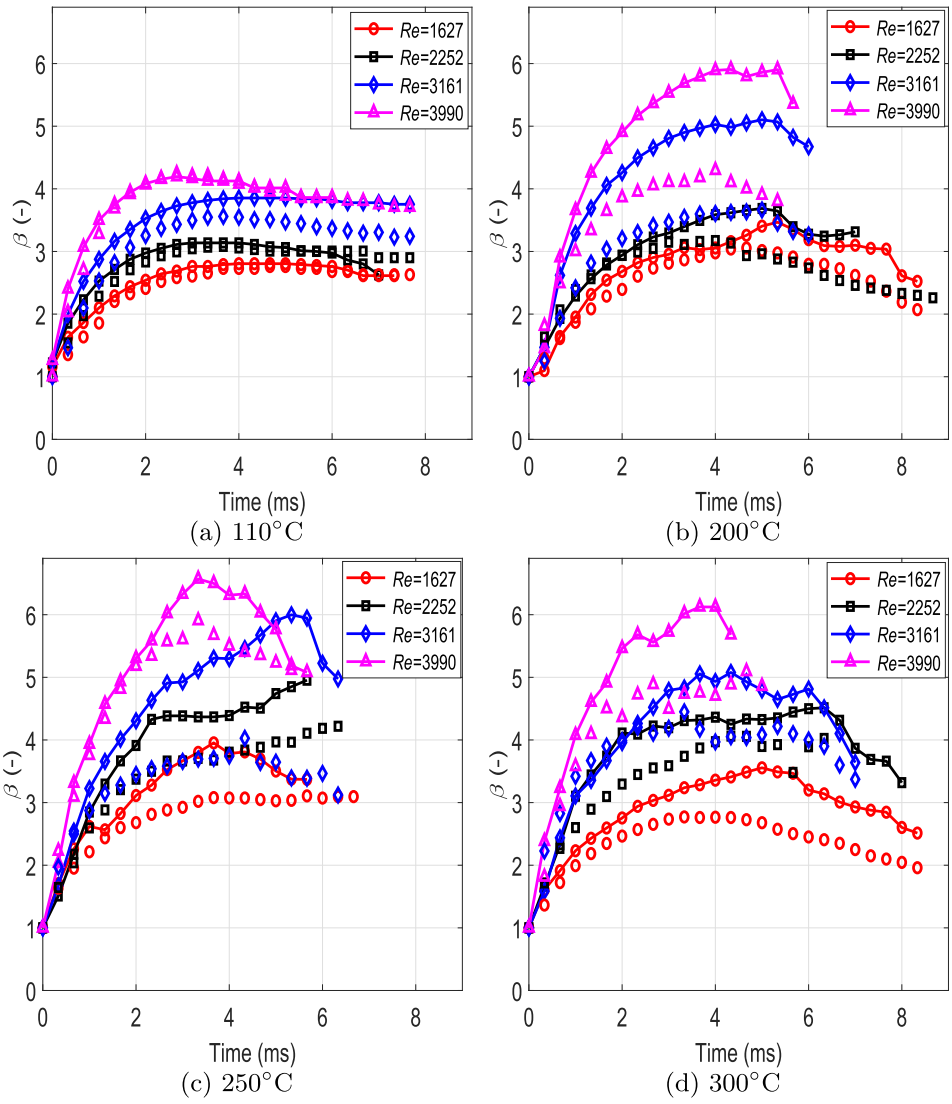

Fig. 7. Comparison of spreading factors of UWS and surfactant-added UWS droplets at various droplet Re under different T_s conditions. Spreading factors of DDA75 droplets were significantly higher compared to UWS droplets under high T_s. Continuous line represents DDA75 droplets and, scattered plot shows spreading of UWS droplets.

Overall, droplet spreading and receding of UWS and DDA75 droplets strongly depends on *Re* number and wall temperatures. Also, the reduction in surface tension of UWS favours droplet spreading and results in higher spreading factors under high T_s conditions, which might enhance the mixing of DDA75 in SCR systems through improved evaporation due to higher surface area.

3.3. Maximum spreading factor, (β_{max})

The maximum spreading factor (β_{max}) is the maximum dispersion of liquid lamella after the impact of droplet and this was obtained by measuring the maximum extent of the spreading lamella using the binary images with the help of image processing methods as explained in 2.2. The effect of surface tension and wall temperature on β_{max} have been studied under different droplet *Re* numbers as shown in Fig. 8. The β_{max} values for considered range of *Re* number for UWS and DDA75 droplets were almost similar (around 3.2% higher for DDA75 droplets) at lower wall temperatures (e.g. T_s = 110 °C), which underlines the marginal influence of surface tension of UWS under these conditions, as discussed in the previous section. More prominent influence of reduction in surface tension of UWS was observed at higher wall temperatures (T_s >200 °C), where β_{max} values of DDA75 droplets were larger by up to 37% compared to that of UWS droplets at both, low and high *Re* conditions. This could be attributed to the Leidenfrost behavior observed at wall temperatures beyond 200 °C, when vapor film formed between the liquid lamella and the hot surface. The formation of vapor film tends to lower the interfacial forces between liquid lamella and the surface, which favoured spreading of the liquid lamella. Also, lower surface tension of DDA75 might have further assisted in droplet spreading, leading to an increase in β_{max} values of DDA75 droplets under higher wall temperature and *Re* number conditions.

The impact of wall temperature on β_{max} was different for UWS and DDA75 droplets. For UWS droplets, the β_{max} values were varying in the range from 2.75 to 3.11 with the increase in wall temperature at low *Re* condition (*Re* = 1627); whereas the significant increase of 39% (from 4.24 to 5.9) in β_{max} was observed at high *Re* condition (*Re* = 3990) when T_s was increased from 110 °C to 250 °C. On the other hand, DDA75 droplets showed a noticeable increase in the β_{max} values under both, low and high *Re* conditions (~ 40% at low *Re* and 56% at high *Re*) with the increase in wall temperature. This might be attributed to the combination of lower surface tension forces and the formation of vapor film under higher wall temperatures, which favours lamella spreading and an increase of β_{max} values of DDA75 droplets even under low *Re* conditions. Thus, higher β_{max} values were observed for DDA75 droplets, particularly

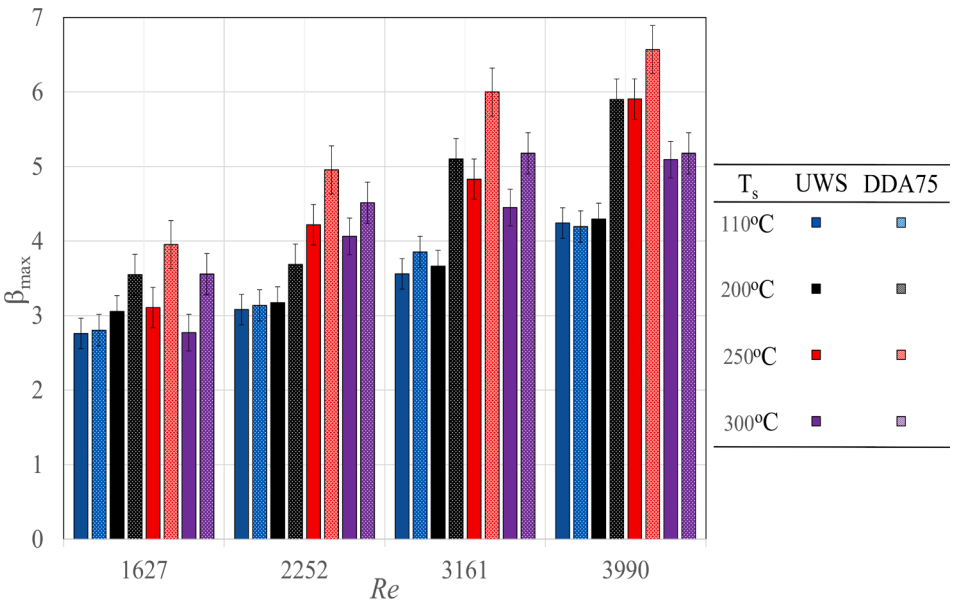

Fig. 8. Maximum spreading factors (β_{max}) of UWS and DDA75 droplets at different wall temperatures. The β_{max} values of UWS droplets strongly depend on *Re*, T_s and surface tension. Solid bars represent UWS droplets, while patterned bars represent DDA75 droplets; the error-bars indicate mean standard error.

at high *Re* conditions and wall temperature more than 200 °C, which helps to achieve improved mixing of DDA75 in SCR systems through better evaporation of DDA75 droplets.

The β_{max} values obtained from the present experimental conditions have been compared to those from various empirical correlations [27,53,54,24];the mathematical expressions for correlations from Bayer and Megaridis [53], Scheller & Bousfield [54] and Pasandideh-Fard et al. [27] are given in Eqs. 1 to 3, respectively:

$$\beta_{max} = 0.72 \cdot (ReWe^{\frac{1}{2}})^{0.14} \quad (1)$$

$$\beta_{max} = 0.61 \cdot (ReWe^{\frac{1}{2}})^{0.166} \quad (2)$$

$$\beta_{max} = 0.5 \cdot Re^{0.25} \quad (3)$$

Fig. 9 presents the comparison of the three empirical correlations with experimental values of UWS and DDA75 droplets at $T_s = 250$ °C. The predictions of these correlations showed considerable deviation with our experimental β_{max} values of UWS and DDA75 droplets, the deviations between the experimental data and predictions were significant at higher *Re* conditions. This deviation could be related to the fact that most of these correlations had been proposed under cold-wall conditions (T_s<T_{sat}) and did not consider the effect of wall temperature on the spreading process. Also, the variations in operating conditions (e.g. T_s and U_0, d_0 etc.), thermo-physical properties of the liquids (viz., saturation temperature, dynamic viscosity and surface tension) and surface properties might have resulted in a limited validity range of these correlations.

The experimental observations reveal that maximum spreading factor of UWS droplets impacting on a hot wall depends on various parameters viz., its thermo-physical properties (e.g. density, ρ_l, surface tension σ_l) and saturation temperature, T_{sat}) and operating conditions (initial droplet diameter (D_0), velocity of the droplet (U_0) and wall temperature) and this can be expressed as:

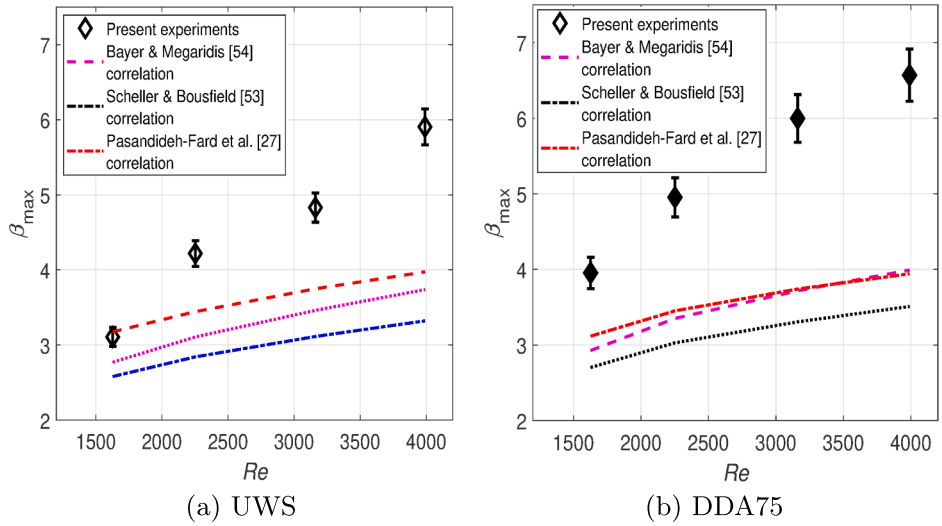

Fig. 9. Comparison of maximum spreading factors of UWS and DDA75 droplets from present experiments with different existing correlations at $T_s = 250$ °C. The correlations of [[27,53,54]] showed significant deviation with the present measurements for both, UWS and DDA75 droplets. Error-bars represent mean standard error in the measurements. Open symbols represent UWS droplets, while filled symbols represent DDA75 droplets.

$$\beta_{max} = f(\rho_l, \sigma_l, D_0, U_0, T_s, T_{sat}) \quad (4)$$

where, T_s and T_{sat} are wall temperature and saturation temperature of UWS in K, respectively. Equation Eq. 4 can be written in non-dimensional form as follows:

$$\beta_{max} = C \cdot We^{a} \cdot \left(\frac{Ts}{T_{sat}}\right)^{b} \quad (5)$$

The coefficient C and the exponent terms a and b in the correlation were obtained using regression analysis and present experimental data and this results in a value of 1.15 for C, and 0.23 and 0.62 for a and b, respectively as shown in Eq. 6.

$$\beta_{max} = 1.15 \cdot We^{0.23} \cdot \left(\frac{Ts}{T_{sat}}\right)^{0.62} \quad (6)$$

The accuracy of the proposed correlation was assessed using a mean error, calculated as a mean of absolute errors, for different liquids including UWS and DDA75 droplets. The validity of the correlation (Eq. 6) and the effect of temperature ratio on prediction of β_{max} values were evaluated by comparing the predicted β_{max} values with the experimental values from current and past studies [[24,55,52,26,56]] and also with the predictions from correlations of [[27,53,54]] under a range of wall temperatures, *Re* and Weber number conditions.

The validity of proposed temperature-dependent correlation (Eq. 6) has been established in Fig. 10 by comparing the experimental values of β_{max} from the various available high-temperature experimental data [[55,52]] with predicted β_{max} values from our correlation. The predicted β_{max} values from correlations proposed in [[27,53,54,24]] under cold-impact and high T_s conditions for different liquids viz., UWS [24], camelina-derived alternative jet fuel [55] and Jatropha biodiesel [52] have also been considered in Fig. 10. The predictions from Bayer & Megaridis [53] correlation and Scheller & Bousfield [54] correlation agreed well with experimental data of UWS and camelina-derived alternative jet fuel droplets under cold-wall conditions (maximum mean error up to ~ 8%) as shown in Fig. 10(a) and (b). However, the predictions of the correlations of [[27,53,54]] showed considerable deviations compared to experimental data under high wall temperature conditions with mean error in the range from 12.66% to 46.44%; the deviations were significant at high wall temperature and high *We*

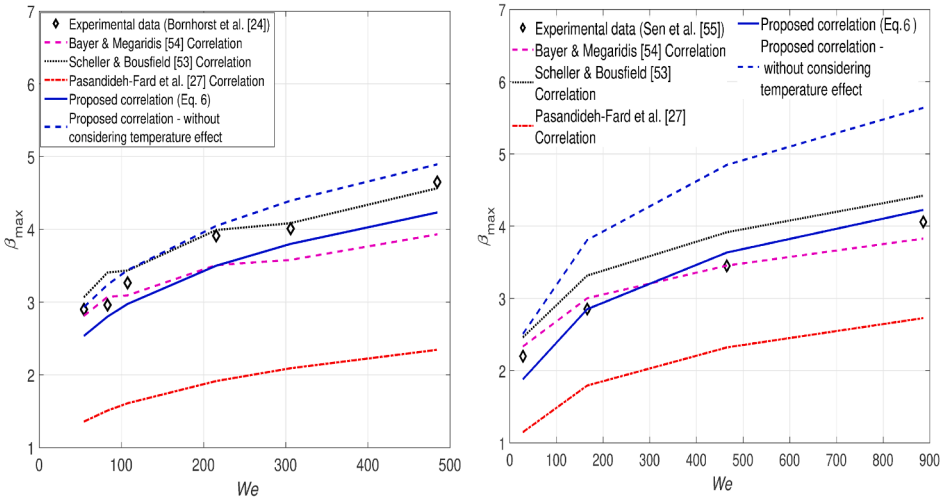

(a) Bornhorst et al. [24]: UWS; T_s=25°C (b) Sen et al. [55]: Camelina-derived alternative jet fuel; T_s=28°C

Under room temperature conditions

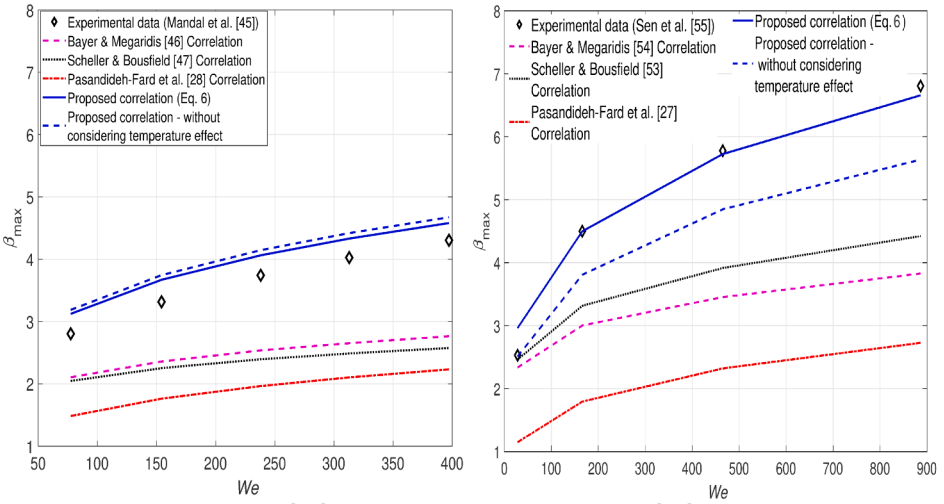

(c) Kumar and Mandal [52]: Jatropha biodiesel; T_s=330°C (d) Sen et al. [55]: Camelina-derived alternative jet fuel; T_s=350°C

Under higher T_s conditions

Fig. 10. Comparison of experimental and predicted β_{max} values from literature [[24,55,52]] with those from predicted values from [[27,53,54]] and those from proposed correlation with and without considering temperature effect under two different T_s conditions for various liquids. The correlations from [[27,53,54]] showed deviations with the experimental data at high T_s conditions. The predictions from proposed correlation (Eq. 6) were in agreement with the experimental values, whereas the proposed correlation showed deviations when temperature effect was not considered.

conditions as can be observed in Fig. 10(c) and (d), this might be attributed to the fact that these correlations have not considered the effect of wall temperature on β_{max} values. On the other hand, predictions from our correlation (Eq. 6) agreed well with the experimental data under high T_s conditions with mean error of 8.1%. Further, the contribution of temperature effect in prediction of β_{max} values was evaluated by neglecting temperature ratio term (i.e. T_s/T_{sat}) in Eq. 6. The predictions of the proposed correlation showed noticeable deviations (mean error up to 31.75%) when temperature effect was not considered. Thus, the temperature ratio (T_s/T_{sat}) has significant contribution in spreading process and can not be neglected in the prediction of β_{max} values. These observations were further confirmed by comparing the experimental β_{max} values of UWS and DDA75 with the predictions of the proposed correlation with and without considering the effect of temperature ratio as shown in Fig. 11. Fig. 11 also provides a comparison of predicted β_{max} values from various empirical correlations [27,53,54,24] with the present experimental β_{max} values of UWS and DDA75 droplets. The most of the predictions from the empirical correlations of [[27,53,54]] showed considerable deviations in range of mean error from 14.24% to 34.47% for both UWS and DDA75 droplets as can be observed in Fig. 11(a) and (b), which might be because of neglecting the effect of temperature on spreading process in these correlations. Further, the contribution of temperature effect in predictions of β_{max} values of UWS and DDA75 droplets was evaluated by neglecting temperature ratio term (i.e. T_s/T_{sat}) in Eq. 6. The predicted β_{max} values of UWS and DDA75 droplets (red square symbols in Fig. 11(a) and (b)) showed considerable deviations, only 43.7% of the predicted values were in the error band of ±15 (mean error ~ 16.75%) when the temperature effect was not considered in our correlation, whereas around 90% predicted β_{max} values were in the error band of ±15 (mean error ~ 8.19%) when the temperature effect was considered. Furthermore, the predicted β_{max} values of UWS and DDA75 from our correlation agreed well with the experimental values under both, cold-wall ($T_s<T_{sat}$) condition from Bornhorst et al. [24] and hot wall conditions ($T_s>T_{sat}$) from the present study, showing a mean error of 9.79% at the cold-wall conditions (Bornhorst et al. [24]) and 8.19% at the hot-wall conditions of the present study, which underlines the influence of temperature ratio on β_{max} values of UWS and DDA75 droplets.

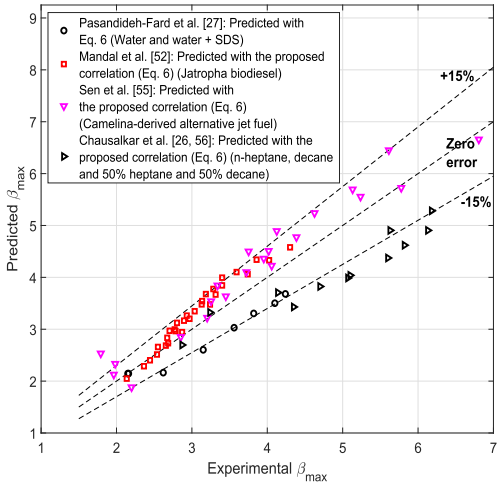

Fig. 12. Comparison of experimental and predicted β_{max} values for various liquids including different fuels i.e. alternative jet fuel, Jatropha biodiesel, n-heptane and n-decane etc. The most of predicted β_{max} values from the proposed correlation were in the error band of ±15%.

The predictions of the proposed correlation were further extended to estimate the β_{max} values of different liquids, including water [27], surfactant-added water [27], hydrocarbon fuels (n-heptane, n-decane etc) [26,56], Jatropha biodiesel [52] and camelina-based alternative jet fuel [55] under a wide range of thermo-physical properties of liquid and operating conditions as shown in Fig. 12. It was observed that most of the β_{max} values (around 87%) from the proposed correlation are within the error band of ±15% with mean error of 10.61%. Table 3 presents the summary of the range of parameters and mean error in predicted β_{max} values for different liquids having wide range of thermo-physical properties, which also confirms the ability of the proposed correlation to predict β_{max} values of UWS and DDA75 droplets under the wide range of wall temperatures, *Re* and Weber number conditions.

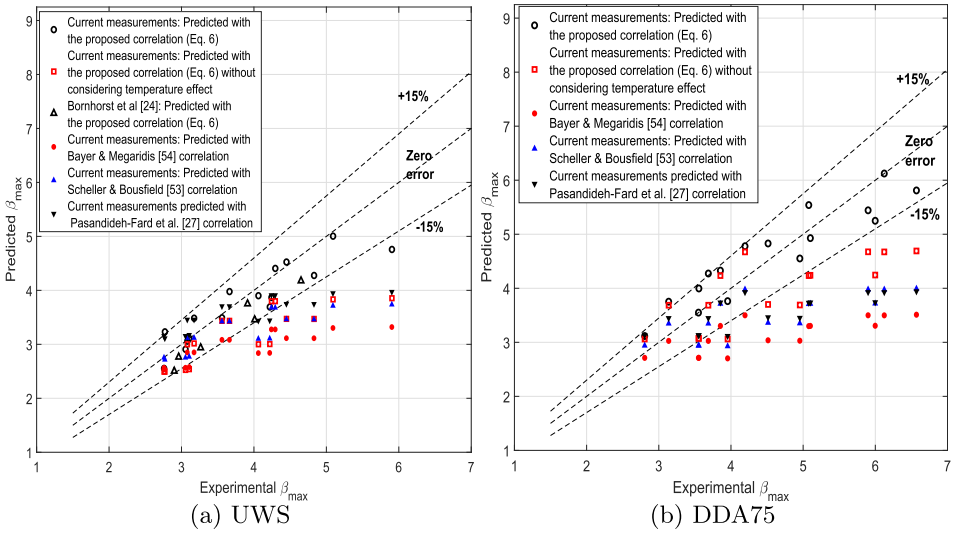

Fig. 11. Comparison of experimental and predicted β_{max} values of UWS and DDA75. The most of predicted β_{max} values from the proposed correlation were in the error band of ±15% whereas the correlations of [[27,53,54]] showed considerable deviations with experimental β_{max} values of current study for UWS and DDA75 droplets. However, the present correlation showed noticeable deviations when the temperature effect was not considered.

Table 3
The range of the parameters and MAPE of the proposed correlation.

Source	Liquid	ρ_l (kg/m^3)	σ_l (mN/m)	D_0 (mm)	U_0 (m/s)	We	T_s (K)	T_{sat} (K)	Mean error (%)
Borhnorst et al. [24]	UWS	1066	72.7	1.95 –2.96	1.39–3.36	54.4–484.3	298.15	385.55	9.79
Pasandideh-Fard et al. [27]	Water and SDS surfactant	1000	72.3–50	0.616–2.07	1–4.28	27–271	298.15	273.15	11.51
Kumar and Mandal [52]	Jatropha biodiesel	898.7	32	2.85	0.99–2.21	78–396	303.15–603.15	623.15	8.41
Sen et al. [55]	Camelina-derived alternative jet fuel	771.9	24.8	2.02–2.48	0.62–3.44	28–886	298.15–623.15	475.75	11.08
Chusalkar et al. [26,56]	n-heptane, n-decane and a mixture of 50% n-heptane and n-decane	20.14–23.8	684–750	1.8	0.8–3.8	27–664	300.15 –573.15	371.65–473.15	14.72
Current study	UWS and DDA75	1066.3–1070.3	73.7–30.2	2.05	1–2	28.94–444.7	383.15–573.15	377.35	8.19

3.4. Droplet size distributions of secondary droplets

Fragmentation of lamella results in the formation of larger secondary droplets of different sizes. The diameters of the secondary droplets were measured using the image processing methods described in Section 2.2. The size distributions of secondary UWS and DDA75 droplets, normalized with an initial droplet diameter (D_0), have been compared in Fig. 13 for two wall temperature conditions viz., T_s = 200 °C and 300 °C. The influence of wall temperature and reduction in surface tension of UWS on the drop-size distributions of secondary droplets have been studied

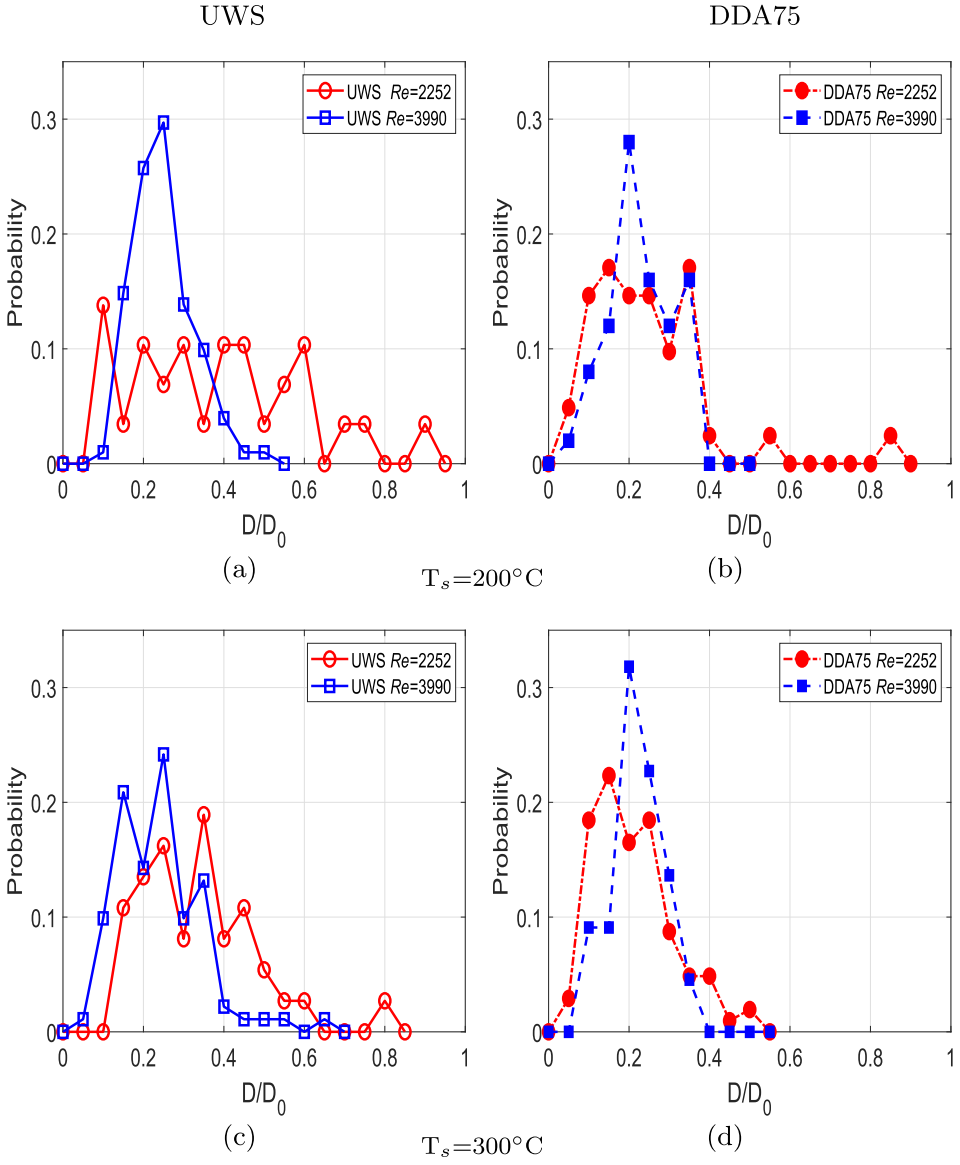

Fig. 13. Drop-size distributions of secondary droplets at two T_s and different Re conditions for UWS and DDA75 droplets. The droplet size distributions became narrower with the increase in *Re* and due to the addition of surfactant to UWS.

for various *Re* conditions. The drop-size distributions of both, UWS and DDA75 droplets became narrower with the increase in *Re* at each wall temperature condition, as shown in Fig. 13(a)–(d). The observed maximum narrowing of size distributions was ~ 36.7% and this was due to higher inertia forces compared to surface tension forces (i.e. higher Weber numbers) that favoured lamella breakup and resulted in smaller droplets. Further, the reduction in surface tension of UWS also has considerable influence on drop-size distributions of secondary droplets. The drop-size distributions of DDA75 droplets were slightly narrower compared to those of UWS droplets at both wall temperature conditions as can be observed in Fig. 13(c) and (d) Also, a reduction in the number of bigger size droplets by up to 35.3% were observed for DDA75 compared to that of UWS. This might be attributed to improved spreading of DDA75 droplets due to reduction in surface tension of UWS, the larger β_{max} values of DDA75 droplets also results in reduced thickness of a spreading lamella. Moreover, lower surface tension of DDA75 droplets leads to significantly higher Weber numbers suggesting weaker surface tension forces compared to inertial forces. Thus, the combination of high β_{max} values and high *We* of DDA75 droplets favours secondary breakup of DDA75 droplets and generated more number of smaller droplets, resulting in narrower drop-size distributions.

The increase in wall temperature also slightly improved droplet size distributions of UWS droplets, showing a marginal reduction in number of bigger size droplets by 9.8% at low *Re* conditions when the wall temperature was increased from 200 °C to 300 °C. Interestingly, the increase in wall temperature favoured breakup of DDA75 lamella significantly, the number of bigger size droplets reduced considerably by up to 36% as shown in Fig. 13(b) and (d). Also, the drop-size distribution of DDA75 droplets became narrower with 80% of its droplets having their sizes smaller than 30% of diameter of the parent droplet along with a very small number of big secondary droplets compared to that of UWS droplets at high wall temperature and high *Re* condition (i.e. $Re = 3990$; $T_s = 300$ °C) as shown in Fig. 13(d). This might be attributed to enhanced breakup of DDA75 lamella due to the combination of higher inertia forces and weak surface tension forces in DDA75 droplets. Moreover, stronger repulsive forces due to Leidenfrost effect at higher wall temperatures might also aid the breakup of DDA75 lamella, resulting in narrower drop-size distributions of secondary DDA75 droplets at high wall temperatures. Thus, higher *Re* and reduction in surface tension of UWS favours narrower drop-size distributions of secondary droplets at high wall temperatures, which enhances mixing of DDA75 with the engine exhaust in urea-SCR systems.

4. Conclusion

This work presents detailed analyses on droplet-wall interaction of a UWS droplet impinging on a hot plate under urea-SCR relevant conditions. Impact of lowering surface tension of UWS on droplet morphology and impact dynamics were explored, this was done by adding N,N, Dimethyldodecylamine N-oxide (DDA) surfactant of 75% of its critical miscelle concentration (CMC) in UWS. The addition of surfactant reduced surface tension of UWS significantly from 73.7 to 30.2 mN/m. The high-speed shadowgraph imaging and analyses of secondary droplets of lamella breakup were performed to quantify the variations in the droplet-sizes caused by varying surface tension of UWS, impact momentum and wall temperature (T_s).

Droplet morphology of UWS and DDA75 droplets revealed distinct modes viz., deposition, rebound and breakup, which were further classified based on the occurrence of thermal atomization. The outcomes of impact of UWS and surfactant-added UWS droplets on a hot surface were summarized in a regime map, which revealed that droplet deposition (for T_s below 150 °C) might result in undesirable urea wall residues in SCR systems even for surfactant-added UWS droplets. Thermal atomization in UWS droplet was observed at different wall temperatures, 150 °C < T_s<250 °C for UWS and 150 °C < T_s<200 °C for DDA75 droplets. A new empirical correlation for thermo-hydrodynamic impact of droplet was developed by incorporating temperature effect to predict maximum spreading factor (β_{max}) of UWS and DDA75 droplets under wide wall temperature conditions, the predictions of the correlation resulted in a mean error of 8.19% with the present experimental measurements and with those data reported in literature and this was 9.79%. The correlation was further extended to predict β_{max} values of different liquids including water, hydrocarbon and alternative fuels viz., n-heptane, n-decane, Jatropha biodiesel and camelina-based alternative jet fuel, the correlation agreed well with past experimental studies with the maximum mean error of 14.72%. Spreading of DDA75 lamella was significantly larger than that of UWS droplets by a maximum of up to 37% due to reduction in surface tension. The drop-size distributions of secondary droplets formed after lamella breakup revealed strong influence of wall temperature, impact momentum and surface tension of UWS, the drop distributions of DDA75 droplets were significantly narrower (up to 36%) compared to those of UWS droplets at high wall temperature and high *Re* conditions with most of the droplets (around 80%) smaller than 30% of initial droplet diameter. This investigation reveals that mixing in urea-SCR systems can be enhanced with the use of surfactant-added UWS through improved evaporation due to higher spreading and narrower drop-size distributions of the secondary droplets and possible lower urea residues due to reduction in surface tension of UWS.

Declaration of Competing Interest

The authors declare that they have no known competing financial interests or personal relationships that could have appeared to influence the work reported in this paper.

Acknowledgments

The authors acknowledge the financial support of Engineering and Physical Sciences Research Council (EPSRC) of the U.K. under Grant No. EP/P031226/1 for this work.

References

[1] Guan B, Zhan R, Lin H, Huang Z. Review of state of the art technologies of selective catalytic reduction of NOx from diesel engine exhaust. Appl Therm Eng 2014;66 (1–2):395–414.
[2] F. Birkhold, U. Meingast, P. Wassermann, O. Deutschmann, Analysis of the injection of urea-water-solution for automotive SCR DeNOx-systems: modeling of two-phase flow and spray/wall-interaction, SAE International Journal of Engines 5 (2006-01-0643) (2006) –.
[3] Liao Y, Furrer R, Eggenschwiler PD, Boulouchos K. Experimental investigation of the heat transfer characteristics of spray/wall interaction in diesel selective catalytic reduction systems. Fuel 2017;190:163–73.
[4] Ebrahimian V, Nicolle A, Habchi C. Detailed modeling of the evaporation and thermal decomposition of urea-water solution in SCR systems. AIChE J 2012;58(7): 1998–2009.
[5] Vignesh R, Ashok B. Critical interpretative review on current outlook and prospects of selective catalytic reduction system for de-nox strategy in compression ignition engine. Fuel 2020;276:117996.
[6] Spiteri A, Eggenschwiler PD, Liao Y, Wigley G, Michalow-Mauke KA, Elsener M, Kröcher O, Boulouchos K. Comparative analysis on the performance of pressure and air-assisted urea injection for selective catalytic reduction of NO_0. Fuel 2015; 161:269–77.
[7] Varna A, Spiteri AC, Wright YM, Eggenschwiler PD, Boulouchos K. Experimental and numerical assessment of impingement and mixing of urea–water sprays for nitric oxide reduction in diesel exhaust. Appl Energy 2015;157:824–37.
[8] Liao Y, Eggenschwiler PD, Rentsch D, Curto F, Boulouchos K. Characterization of the urea-water spray impingement in diesel selective catalytic reduction systems. Appl Energy 2017;205:964–75.
[9] Pratama RH, Moon S, Kim H-H, Oguma M. Application of electrostatic force for the atomization improvement of urea-water sprays in diesel SCR systems. Fuel 2019; 116571.
[10] Postrioti L, Brizi G, Ungaro C, Mosser M, Bianconi F. A methodology to investigate the behaviour of urea-water sprays in high temperature air flow for SCR de- NOx applications. Fuel 2015;150:548–57.
[11] Payri R, Bracho G, Gimeno J, Moreno A. Investigation of the urea-water solution atomization process in engine exhaust-like conditions. Exp Therm Fluid Sci 2019; 108:75–84.

[12] Kapusta ŁJ, Sutkowski M, Rogóż R, Zommara M, Teodorczyk A. Characteristics of water and urea–water solution sprays. Catalysts 2019;9(9):750.
[13] Oh J, Lee K. Spray characteristics of a urea solution injector and optimal mixer location to improve droplet uniformity and NOx conversion efficiency for selective catalytic reduction. Fuel 2014;119:90–7.
[14] M. Lecompte, S. Raux, A. Frobert, Experimental characterization of SCR DeNOx systems: Visualization of urea-water-solution and exhaust gas mixture, in: SAE Technical Paper, no. 2014-01-1524, SAE International, 2014.
[15] Zhang C, Sun C, Wu M, Lu K. Optimisation design of scr mixer for improving deposit performance at low temperatures. Fuel 2019;237:465–74.
[16] Dörnhöfer J, Börnhorst M, Ates C, Samkhaniani N, Pfeil J, Wörner M, Koch R, Bauer H-J, Deutschmann O, Frohnapfel B, et al. A holistic view on urea injection for no x emission control: Impingement, re-atomization, and deposit formation. Emission Control Sci Technol 2020:1–16.
[17] Schweigert D, Damson B, Lüders H, Stephan P, Deutschmann O. The effect of wetting characteristics, thermophysical properties, and roughness on spray-wall heat transfer in selective catalytic reduction systems. Int J Heat Mass Transfer 2020;152:119554.
[18] Huang H, Chen Y, Li Z, Wang H, Hao B, Chen Y, Lei H, Guo X. Analysis of deposit formation mechanism and structure optimization in urea-SCR system of diesel engine. Fuel 2020;265:116941.
[19] Liang G, Mudawar I. Review of drop impact on heated walls. Int J Heat Mass Transfer 2017;106:103–26.
[20] Yarin AL. Drop impact dynamics: splashing, spreading, receding, bouncing. Annu Rev Fluid Mech 2006;38:159–92.
[21] Moreira A, Moita A, Panao M. Advances and challenges in explaining fuel spray impingement: How much of single droplet impact research is useful? Prog Energy Combust Sci 2010;36(5):554–80.
[22] Y. Qiao, S. Chandra, Experiments on adding a surfactant to water drops boiling on a hot surface, Proc R Soc London Ser A 453 (1959) (1997) 673–689.
[23] Bertola V. An impact regime map for water drops impacting on heated surfaces. Int J Heat Mass Transfer 2015;85:430–7.
[24] Börnhorst M, Cai X, Wörner M, Deutschmann O. Maximum spreading of urea water solution during drop impingement. Chem Eng Technol 2019;42(11):2419–27.
[25] Roisman I, Breitenbach J, Tropea C. Thermal atomisation of a liquid drop after impact onto a hot substrate. J Fluid Mech 2018;842:87.
[26] Chausalkar A, Kong S-C, Michael JB. Multicomponent drop breakup during impact with heated walls. Int J Heat Mass Transfer 2019;141:685–95.
[27] Pasandideh-Fard M, Qiao Y, Chandra S, Mostaghimi J. Capillary effects during droplet impact on a solid surface. Phys Fluids 1996;8(3):650–9.
[28] A. Chausalkar, C.-B.M. Kweon, J.B. Michael, Multi-component fuel drop-wall interactions at high ambient pressures, Fuel 283, 119071.
[29] F. Birkhold, Selektive katalytische reduktion von stickoxiden in kraftfahrzeugen: Untersuchung der einspritzung von harnstoffwasserlösung, PhD thesis, Karlsruher Institut für Technologie, Karlsruhe, Germany, 2007.
[30] D. Kuhnke, Spray/wall interaction modelling by dimensionless data analysis, PhD thesis, Aachen, Germany, 2004.
[31] Börnhorst M, Deutschmann O. Single droplet impingement of urea water solution on a heated substrate. Int J Heat Fluid Flow 2018;69:55–61.
[32] M. Quissek, T. Lauer, O. García-Afonso, S. Fowles, Identification of film breakup for a liquid urea-water-solution and application to cfd, SAE Technical Paper, 2019-01-0983.
[33] Terzis A, Kirsch M, Vaikuntanathan V, Geppert A, Lamanna G, Weigand B. Splashing characteristics of diesel exhaust fluid (adblue) droplets impacting on urea-water solution films. Exp Therm Fluid Sci 2019;102:152–62.
[34] Wu Y, Wang Q, Zhao C. Three-dimensional droplet splashing dynamics measurement with a stereoscopic shadowgraph system. Int J Heat Fluid Flow 2020;83:108576.
[35] Bertola V. Drop impact on a hot surface: effect of a polymer additive. Exp Fluids 2004;37(5):653–64.
[36] Gatne KP, Jog MA, Manglik RM. Surfactant-induced modification of low weber number droplet impact dynamics. Langmuir 2009;25(14):8122–30.
[37] Aytouna M, Bartolo D, Wegdam G, Bonn D, Rafaï S. Impact dynamics of surfactant laden drops: dynamic surface tension effects. Exp Fluids 2010;48(1):49–57.
[38] Alizadeh A, Bahadur V, Zhong S, Shang W, Li R, Ruud J, Yamada M, Ge L, Dhinojwala A, Sohal M. Temperature dependent droplet impact dynamics on flat and textured surfaces. Appl Phys Lett 2012;100(11):111601.
[39] Chen H, Cheng W-L, Peng Y-H, Jiang L-J. Dynamic leidenfrost temperature increase of impacting droplets containing high-alcohol surfactant. Int J Heat Mass Transfer 2018;118:1160–8.
[40] Cossali G, Marengo M, Santini M. Secondary atomisation produced by single drop vertical impacts onto heated surfaces. Exp Therm Fluid Sci 2005;29(8):937–46.
[41] Tran T, Staat HJ, Prosperetti A, Sun C, Lohse D. Drop impact on superheated surfaces. Phys Rev Lett 2012;108(3):036101.
[42] Ayoub M, Irfan MF, Yoo K-S. Surfactants as additives for NOx reduction during sncr process with urea solution as reducing agent. Energy Convers Manage 2011;52(10):3083–8.
[43] G. Wasow, E. O. Strutz, Method for minimizing the diameter of a urea solution, urea solution and use of a surfactant in urea solution, US Patent 9,050,560 B2 (Apr. 7 2015).
[44] Blaisot J, Yon J. Droplet size and morphology characterization for dense sprays by image processing: application to the diesel spray. Exp Fluids 2005;39(6):977–94.
[45] Kulkarni AP, Deshmukh D. Spatial drop-sizing in airblast atomization – an experimental study. Atomization Sprays 2017;27(11):949–61.
[46] Kulkarni AP, Megaritis T, Ganippa LC. Insights on the morphology of air-assisted breakup of urea-water-solution sprays for varying surface tension. Int J Multiphase Flow 2020;103448.
[47] P. Ayyappan, D. Dou, T. M. Harris, Diesel exhaust fluid formulation that reduces urea deposits in exhaust systems, US Patent 8,999,277 (Apr. 7 2015).
[48] Marengo M, Antonini C, Roisman IV, Tropea C. Drop collisions with simple and complex surfaces. Curr Opin Colloid Interface Sci 2011;16(4):292–302.
[49] Breitenbach J, Kissing J, Roisman IV, Tropea C. Characterization of secondary droplets during thermal atomization regime. Exp Therm Fluid Sci 2018;98:516–22.
[50] Bertola V, Sefiane K. Controlling secondary atomization during drop impact on hot surfaces by polymer additives. Phys Fluids 2005;17(10):108104.
[51] Bhat M, Sivakumar D. Post-spreading behavior of impacting fuel drops on stainless steel surface. Exp Thermal Fluid Sci 2019;102:74–80.
[52] Kumar A, Mandal DK. Influence of the surface temperature on the spreading and receding dynamics of an impacting biodiesel drop. Heat Mass Transfer 2020;56(2):445–57.
[53] Bayer IS, Megaridis CM. Contact angle dynamics in droplets impacting on flat surfaces with different wetting characteristics. J Fluid Mech 2006;558:415.
[54] Scheller BL, Bousfield DW. Newtonian drop impact with a solid surface. AIChE J 1995;41(6):1357–67.
[55] Sen S, Vaikuntanathan V, Sivakumar D. Impact dynamics of alternative jet fuel drops on heated stainless steel surface. Int J Therm Sci 2017;121:99–110.
[56] Chausalkar A, Kweon C-BM, Kong S-C, Michael JB. Leidenfrost behavior in drop-wall impacts at combustor-relevant ambient pressures. Int J Heat Mass Transfer 2020;153:119571.